CRS-stack-based seismic imaging for land data and complex near-surface conditions

Zeno Heilmann and Ingo Koglin, Geophysical Institute, University of Karlsruhe, Germany

Copyright 2005, SBGf – Sociedade Brasiliera de Geofísica

This paper was prepared for presentation at the 9th International Congress of The Brazilian Geophysical Society held in Salvador, Brazil, September 11-14 2005.

Contents of this paper was reviewed by The Technical Committee of the 9th International Congress of The Brazilian Geophysical Society and does not necessarily represent any position of the SBGf, its officers or members. Electronic reproduction, or storage of any part of this paper for commercial purposes without the written consent of The Brazilian Geophysical Society is prohibited.

Summary

In the current situation of rapidly growing demand in oil and gas, on-shore exploration, even under difficult conditions, becomes again more and more important. Unfortunately, rough top-surface topography and a strongly varying weathering layer often result in poor data quality, which makes conventional data processing very difficult to apply.
As recent case studies demonstrated, the Common-Reflection-Surface (CRS) stack produces reliable stack sections with high resolution and superior signal-to-noise ratio compared to conventional methods. Particularly for land data, the increased computational expense required by the generalized high-density velocity analysis preceding the CRS stacking process may be worthwhile. In order to define optimal *spatial* stacking operators, the CRS stack extracts for every sample of the zero offset (ZO) section an entire set of physically interpretable stacking parameters. These so-called *kinematic wavefield attributes*, obtained as a by-product of the data-driven stacking process, can be applied to solve various dynamic and kinematic stacking, modeling, and inversion problems. By this means, a very flexible CRS-stack-based seismic reflection imaging workflow can be established. Besides the CRS stack itself, the main steps of this processing workflow are residual static correction, the determination of a macrovelocity model via tomographic inversion and limited aperture Kirchhoff migration.
The presented extention of the CRS-stack-based imaging workflow provides support for arbitrary top-surface topography. The CRS stack is applied to the original prestack data without the need of any elevation statics. Finally, a redatuming procedure relates the CRS-stacked ZO section, the kinematic wavefield attribute sections, and the quality control sections to a chosen planar measurement level. Thus, an ideal input for a preliminary interpretation and subsequent CRS-stack-based processing steps is provided.

Introduction

Obtaining a sufficiently accurate image, either in time or in depth domain, is often a difficult task in regions governed by complex geological structures and/or complicated near surface conditions. Under such circumstances, where simple model assumptions may fail, it is of particular importance to extract as much information as possible directly from the measured data. Fortunately, the ongoing increase in available computing power makes so-called data-driven approaches (see, e. g., Hubral, 1999) feasible which, thus, have increasingly gained in relevance during the last years. The Common-Reflection-Surface (CRS) stack (see, e. g., Mann, 2002) is one of these promising methods. Besides an improved zero-offset (ZO) simulation, its decisive advantage over conventional methods is that for every ZO sample several, so-called, kinematic wavefield attributes are obtained as a by-product of the data-driven stacking process. As will be shown, they can be applied both to improve the stack itself and to support subsequent processing steps. Using these *CRS attributes*, an advanced data-processing workflow can be established (see, e. g., Heilmann et al., 2004, and references therein) leading from time to depth domain, covering a broad range of seismic reflection imaging issues in a consistent manner. The major steps of this workflow are displayed in Figure 1.

So far, this workflow was limited to data acquired on a planar measurement surface or at least to data for which a planar measurement surface had been simulated by means of elevation statics. However, conventional elevation statics may introduce a certain error to the stack and—even worse—to the CRS attribute sections, as a vertical emergence of every ray has to be assumed. In case of rough top-surface topography this can significantly deteriorate the results of the CRS stack and of all succeeding processing steps. This abstract focuses on an sophisticated integration of topography handling into this CRS-stack-based imaging workflow. Final results of its practical application to a realistic synthetic data set with strong topographic influences and complex near-surface conditions will be shown in our presentation.

CRS stack for topography

In recent years, two different CRS stacking operators that consider the top-surface topography have been developed at Karlsruhe University:

I. Chira and Hubral (2003) and Heilmann (2003) assume a smoothly curved measurement surface. The elevation of all source and receiver locations contributing to a single stacking process are approximated by a parabola defined by the local curvature K_0 and the local dip α_0 of the measurement surface within the considered stacking aperture. This results in a CRS traveltime approximation that reads:

$$\begin{aligned}\tau^2(\Delta m_x, h_x)^{\mathrm{ZO}} \quad = \quad & \left(\tau_0 + \frac{2\,\Delta m_x}{v_0\,\cos\alpha_0}\,\sin(\beta_0-\alpha_0)\right)^2 \\ & + \frac{2\,\tau_0\,\Delta m_x^2}{v_0\,\cos^2\alpha_0}\,\left(K_{\mathrm{N}}\,\cos^2(\beta_0-\alpha_0) - K_0\,\cos(\beta_0-\alpha_0)\right) \\ & + \frac{2\,\tau_0\,h_x^2}{v_0\,\cos^2\alpha_0}\,\left(K_{\mathrm{NIP}}\,\cos^2(\beta_0-\alpha_0) - K_0\,\cos(\beta_0-\alpha_0)\right)\,,\end{aligned} \tag{1}$$

It describes the traveltime along a paraxial ray character-

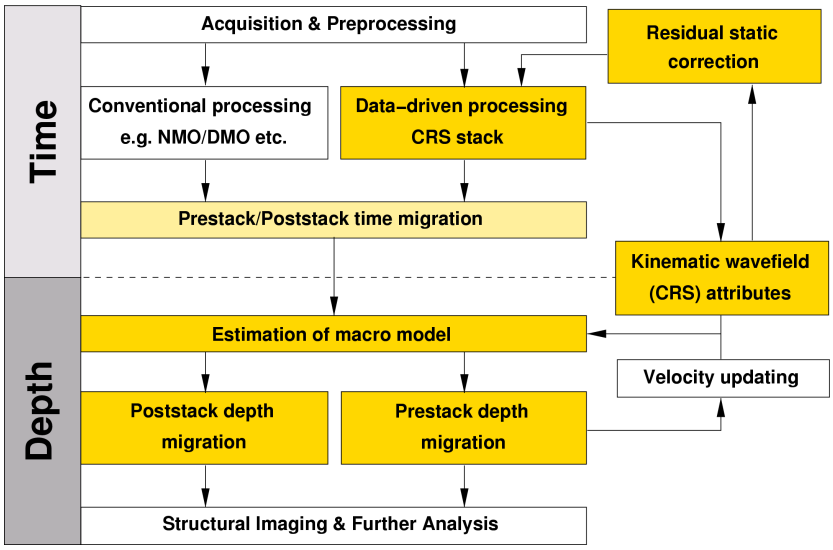

Figure 1: Major steps of seismic-reflection data processing in time and depth domain. CRS-stack-based imaging procedures are highlighted in yellow.

ized by the x-components of midpoint displacement $\Delta\vec{m} = \vec{m} - \vec{m}_{x_0}$ and half-offset $\vec{h}$ in terms of the traveltime τ_0 along the central normal ray emerging at x_0, the near-surface velocity v_0, and the wavefield attributes β_0, R_{NIP}, and R_{N}. The latter three are related to the propagation direction and wavefront curvatures of two hypothetical waves, namely the so-called NIP and normal wave, respectively (Hubral, 1983). Similar to a conventional stacking velocity analysis, the optimum wavefield attributes for each location (x_0, τ_0) are determined automatically by means of coherence analysis. Note, however, that this analysis is carried out with a spatial operator in a multi-dimensional parameter domain. The final results are entire sections of the wavefield attributes β_0, R_{NIP}, and R_{N}, as well as coherence section. For details we refer, e. g., to Jäger et al. (2001).

II. In Zhang (2003) a CRS stacking operator was presented that directly considers the true elevation of every source and receiver. This very general CRS traveltime approximation reads:

$$\begin{aligned}\tau^2(\Delta\vec{m},\vec{h})^{\mathrm{ZO}} &= \left(\tau_0 - \frac{2}{v_0}\,(\Delta m_x \sin\beta_0 + \Delta m_z \cos\beta_0)\right)^2 \\ &+ \frac{2\,\tau_0\,K_{\mathrm{N}}}{v_0}\,(\Delta m_x \cos\beta_0 - \Delta m_z \sin\beta_0)^2 \\ &+ \frac{2\,\tau_0\,K_{\mathrm{NIP}}}{v_0}\,(h_x \cos\beta_0 - h_z \sin\beta_0)^2\,, \qquad (2)\end{aligned}$$

where $(\Delta m_x, \Delta m_z)$ and (h_x, h_z) are the components of midpoint displacement $\Delta\vec{m}$ and half-offset $\vec{h}$ of the considered paraxial ray.

The first approach is attractive from the computational point of view as it is possible to adopt most parts of the conventional CRS stack implementation. In particular, the pragmatic CRS-attribute search strategy using three one-parameter searches to determine the optimal stacking operator can be maintained. However, small elevation statics are still required in order to transfer the original data to the chosen smoothly curved measurement surface. The second approach demands far more computational effort, as two of the three attributes have to be searched simultaneously due to the higher complexity of the stacking operator. On the other hand, no elevation statics are required and the z-coordinate of the emergence points of the simulated ZO rays can be chosen arbitrarily. Promissing results of this approach were presented in Zhang and Wu (2004).

Following the idea of a step-by-step refinement, we chose an implementation that combines both methods of topography handling mentioned above to a cascaded processing strategy. Doing this, most of the specific disadvantages of the single approaches can be compensated without loosing their individual benefits. In a final step, we relate the CRS stack results to a planar reference level above the actual measurement surface. This is done by introducing a fictitious homogeneous top-layer and utilizing the extracted emergence angle β_0 of the simulated ZO rays to extrapolate them up to the reference level. By this redatuming procedure a seamless transition to the tomographic inversion and other succeeding processing steps is provided. Since the reference level lies above the actual measurement surface, the influence of the topography might still be visible in the time domain images, but should disappear after depth migration.

Residual static correction by means of CRS attributes.

The CRS-stack-based residual static correction (RSC) methodology (see, e.g., Koglin and Ewig, 2003) is an iterative process close to the super-trace cross-correlation method by Ronen and Claerbout (1985). In our approach, the cross correlations are performed within CRS supergathers of moveout corrected prestack traces instead of being confined to single common midpoint (CMP), common-shot (CS) or common-receiver (CR) gathers. The moveout correction makes use of the previously obtained CRS attributes and considers the true source and receiver elevations. Thus, elevation static correction can be omitted that may introduce, in certain cases, non surface-consistent errors of the same scale as the searched-for residual statics. Due to the spatial extent of the CRS operator, the CRS supergathers contain many neighboring CMP gathers but

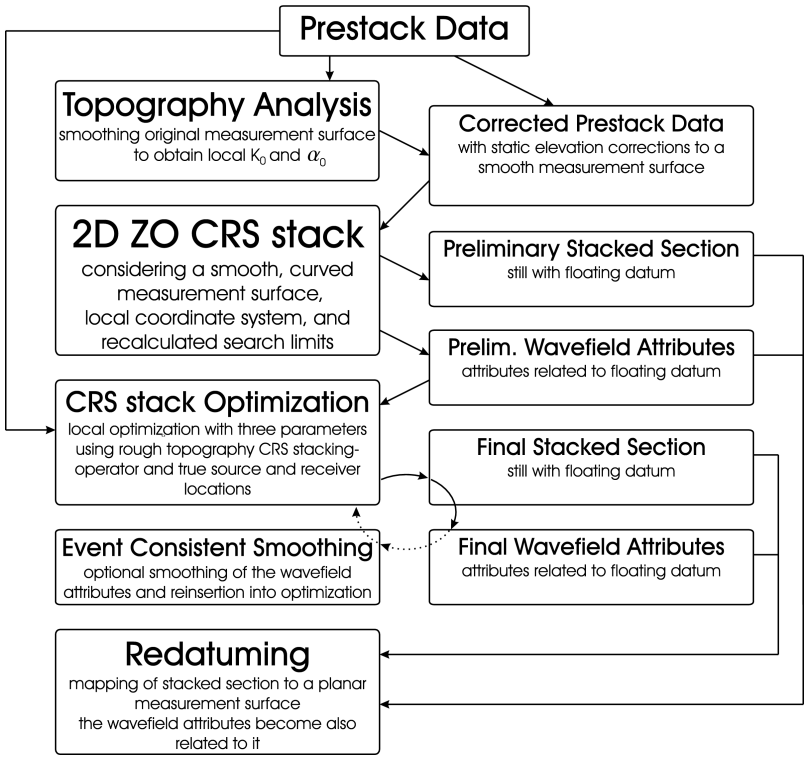

Figure 2: *Sketch of the extended CRS stack method for handling measurement surfaces with topography.*

with different moveout corrections depending on the current ZO location. Thus, the cross correlations of the stacked trace (here used as pilot trace) and the moveout corrected prestack traces are summed up for CS and CR locations. This summation is performed for all CRS supergathers contained in the specified target zone. After all cross correlations are summed up, the searched-for residual time shifts are most likely associated with maxima in the cross correlation stacks. Finally, the estimated time shifts are used to correct the prestack traces and the next iteration of RSC can be started. Therefore, the local three-parameter optimization of the CRS stack is repeated, now using the corrected prestack data set. First results of the CRS stack after three iterations of RSC are depicted in Figures 6 and 7.

CRS moveout correction. To correct for the CRS moveout, the half-offset $\vec{h}$ and midpoint $\Delta\vec{m}$ dependency of equation (2) has to be eliminated. Therefore, the CRS attributes of every time sample are required. These attributes are provided by the attribute search of the first CRS stack applied. With the knowledge of these attributes, each reflection event can be approximately transformed into a horizontal plane at time τ_0 by subtracting the moveout given by

$$\Delta\tau(\Delta\vec{m},\vec{h}) = \tau(\Delta\vec{m},\vec{h}) - \tau_0\,, \tag{3}$$

where τ_0 is given by the considered time sample of the simulated ZO section. This correction is performed for all τ_0 given by each simulated ZO trace of the CRS stack. The result for one ZO trace is called CRS super gather and contains all CRS-moveout-corrected prestack traces which lie inside the corresponding CRS aperture. Thus, the prestack traces are multiply contained in the CRS super gathers but with different moveout corrections in each CRS super gather.

Cross correlation. The cross correlations are performed between every single moveout-corrected trace of each CRS super gather and the corresponding trace of the simulated ZO section, i. e., the pilot trace. Afterwards, all correlation results that belong to the same source or receiver location are summed up. Finally, the residual static value is assumed to be associated with the time shift of the global maxima of the summed correlation results. Our tests have shown that the positive lobe of the correlation result is not always symmetrical around a maxima. Thus, another method is to take a user-defined percentage of the global or local maximum closest to a zero time shift as a minimum threshold and take the center of this area within the positive lobe as the estimated time shift. Additionally, the tapering effect of cross correlations can be compensated. Therefore, the windows of pilot and moveout corrected traces to be correlated are enlarged by the maximum shift. Thus, during the correlation no value is zeroed out before and no tapering effect is contained. Furthermore, a normalization before the correlation in the same way as in the CRS-attribute search (see Mann, 2002) can be applied to weight the traces against each other. Another normalization after the correlation based on its power can be applied before the correlation stack to balance the influence of each contribution. Both normalizations were applied in this case leading to significantly improved results.

Iterations. After the residual static values are obtained from the cross correlation results, the prestack traces are time shifted with the corresponding total time shifts. The total time shift is simply the sum of the corresponding source and receiver static values of each prestack trace. If the CRS stack of these corrected prestack traces is not yet satisfactory, the entire procedure can be started again in two differ-

ent ways with the previously corrected prestack traces. The difference of both ways is that one omits the CRS search for the attributes whereas the other does not. As the CRS search for the attributes is the most time consuming step of our method, it is attractive to omit this step. But on the other hand, it might be dangerous to rely on CRS attributes determined for the uncorrected data: if the time shifts between neighboring traces are too large, the CRS stack probably fails to detect actually contiguous events and their corresponding attributes.

Synthetic data example.

The synthetic data set presented in this abstract was kindly provided by J. A. Dellinger (BP). Figure 3 shows the underlying velocity model, simulating a situation typical for the Canadian overthrust front. Looking at the measurement surface silhouetted against the red background a foothill like topography with rapid changes in elevation can be observed. A magnified view of this topography is shown in Figure 4. The smoothed surface depicted in light green was used as floating reference datum for the CRS stack results. The planar surface (blue) indicates the horizontal reference datum to which these results were subsequently mapped by the redatuming prozedure. For the fictitious layer between the floating datum and the horizontal reference level a constant velocity of 3300 m/s was chosen.
At the right hand side of the model we have a very complex subsurface structure with large velocity contrasts and several velocity inversions. Also the near-surface velocity is subject to strong fluctuations ranging from 2.5 km/s to nearly 6.0 km/s. To account for this fluctuations, the average value of the near-surface velocity within the respective stacking aperture was used for attribute determination, stacking and RSC. The near-surface velocity and its laterally averaged value are depicted in Figure 5. The latter was used for v_0 in Equations 1 (initial CRS stack) and 2 (optimization and RSC). First results of the CRS stack before and after redatuming are depicted in Figures 6 and 7.

Conclusions and Outlook

We presented a recent extension of CRS-stack based imaging adapted to the specific needs of land-data processing. It was shown, how top-surface topography handling can be integrated into the processing workflow in a consistent manner using a CRS-attribute based redatuming procedure that relates the resulting stack and attribute sections to a horizontal reference datum.
So far, the near-surface velocity was assumed to be constant for the entire survey. Our current research focuses on considering a laterally variable near-surface velocity, since both, the kinematic wavefield attributes determined during the initial search and the CRS stack operator used for the final optimization strongly depend on this parameter.
First results for a complex synthetic data set have been presented in this abstract. Besides the influence of the topography the variable near-surface velocity was considered both for the CRS stack itself and for the residual static correction. Results of redatuming the CRS attribute sections as well as results of the tomographic inversion and subsequent limited aperture Kirchhoff pre- and/or poststack depth migration will be shown in the related presentation. The practical application to a real data set is under current development.

Acknowledgments

We would like to thank the sponsors of the Wave Inversion Technology (WIT) Consortium for their support and we gratefully acknowledge S. Gray for creating the synthetic dataset used for this abstract.

References

Chira, P. and Hubral, P. (2003). Traveltime formulas of near-zero-offset primary reflections for curved 2D measurement surface. *Geophysics*, 68(1):255–261.

Duveneck, E. (2004). Velocity model estimation with data-derived wavefront attributes. *Geophysics*, 69(1):265–274.

Heilmann, Z. (2003). Extensions of the Common-Reflection-Surface Stack Considering the Surface Topography and the Near-Surface Velocity Gradient. In *Ext. Abstr., 8th International Congress, Soc. Bras. Geofísica (SBGf), Rio de Janeiro*.

Heilmann, Z., Mann, J., Duveneck, E., and Hertweck, T. (2004). CRS-stack-based seismic reflection imaging - a real data example. In *Extended Abstracts, 66th EAGE Conference and Exhibition, Paris, France*, Session: P211.

Hubral, P. (1983). Computing true amplitude reflections in a laterally inhomogeneous earth. *Geophysics*, 48(8):1051–1062.

Hubral, P., editor (1999). *Special Issue on Macro-Model Independent Seismic Reflection Imaging*, volume 42(3,4) of *Journal of Applied Geophysics*, Amsterdam. Elsevier.

Jäger, C., Hertweck, T., and Spinner, M. (2003). True-amplitude Kirchhoff migration from topography. In *Extended Abstracts*, Session MIG 2.1. Soc. of Expl. Geophys.

Jäger, R., Mann, J., Höcht, G., and Hubral, P. (2001). Common-Reflection-Surface stack: image and attributes. *Geophysics*, 66(1):97–109.

Koglin, I. and Ewig, E. (2003). Residual Static Correction by Means of Kinematic Wavefield Attributes. In *Extended Abstracts*, Session D18. Eur. Assn. Geosci. Eng.

Mann, J. (2002). *Extensions and applications of the Common-Reflection-Surface stack method*. Logos Verlag, Berlin.

Ronen, J. and Claerbout, J. F. (1985). Surface-consistent residual statics estimation by stack-power maximization. *Geophysics*, 50(12):2759 – 2767.

Zhang, Y. (2003). *Common-Reflection-Surface Stack and the Handling of Top Surface Topography*. Logos Verlag, Berlin.

Zhang, Y. and Wu, R. (2004). CRS stack and redatuming for rugged surface topography: a synthetic data example. In *Ext. Abstr., 74th Annual Internat. Mtg., Soc. Expl. Geophys.*, Session: SP4.6.

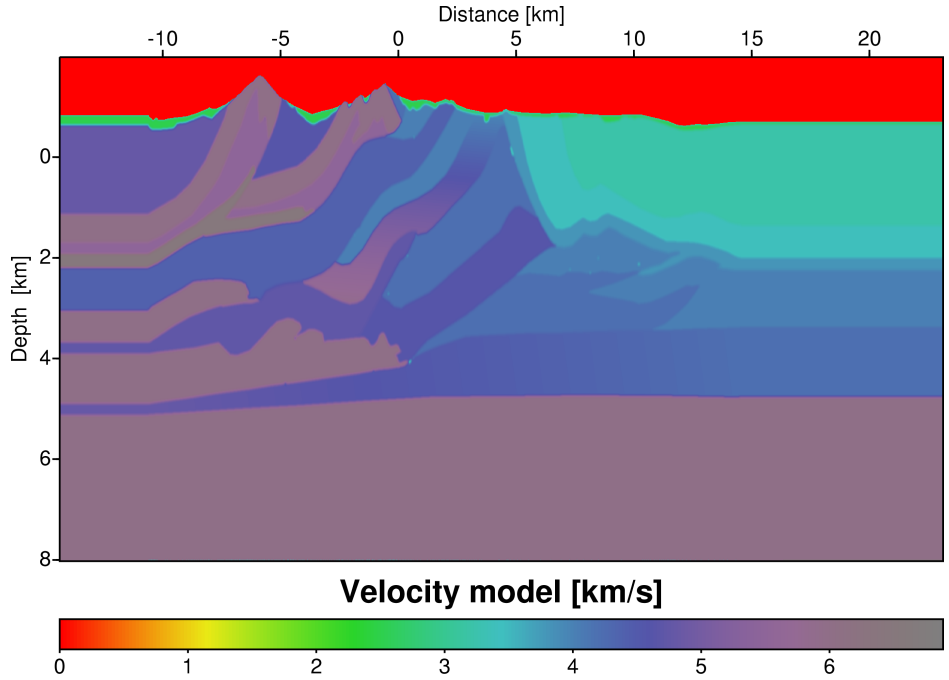

Figure 3: *Velocity model used to generate the prestack data.*

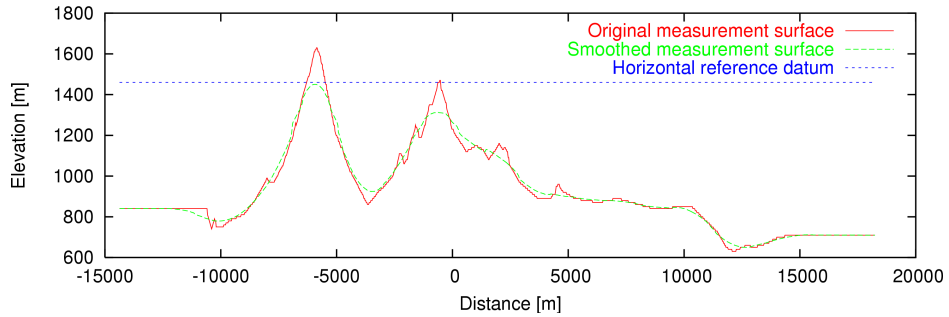

Figure 4: *Comparison between original and smoothed measurement surface. The horizontal surface at* $z = 1460m$ *was used as reference level for the redatuming.*

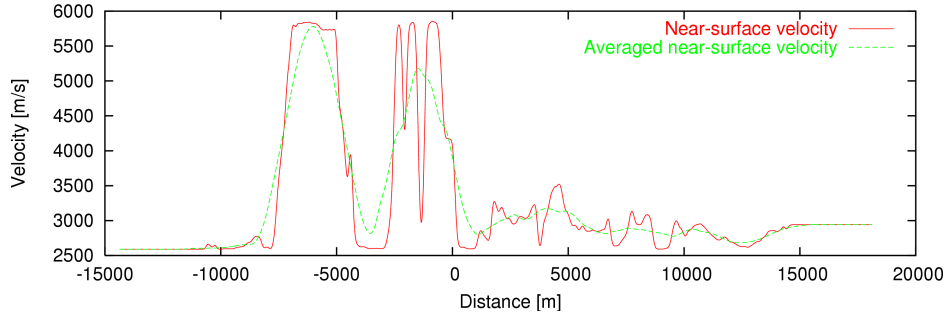

Figure 5: *Comparison between local near-surface velocity and laterally averaged near-surface velocity. To extract the local near-surface velocity from the velocity model given by Figure 4 an (vertically) averaged velocity up to a maximum depth of 80m was calculated.*

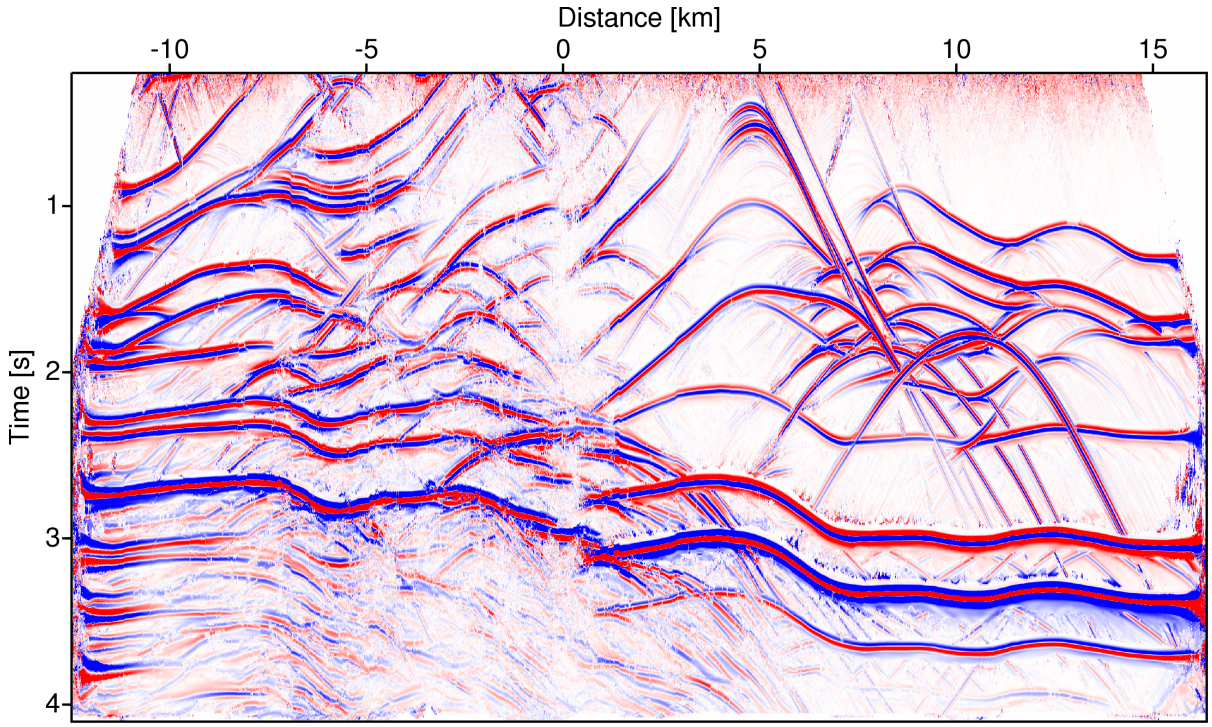

Figure 6: Optimized CRS stack result after three iterations of residual static correction. The simulated ZO traveltimes are related to the smoothed reference surface depicted in Figure 4.

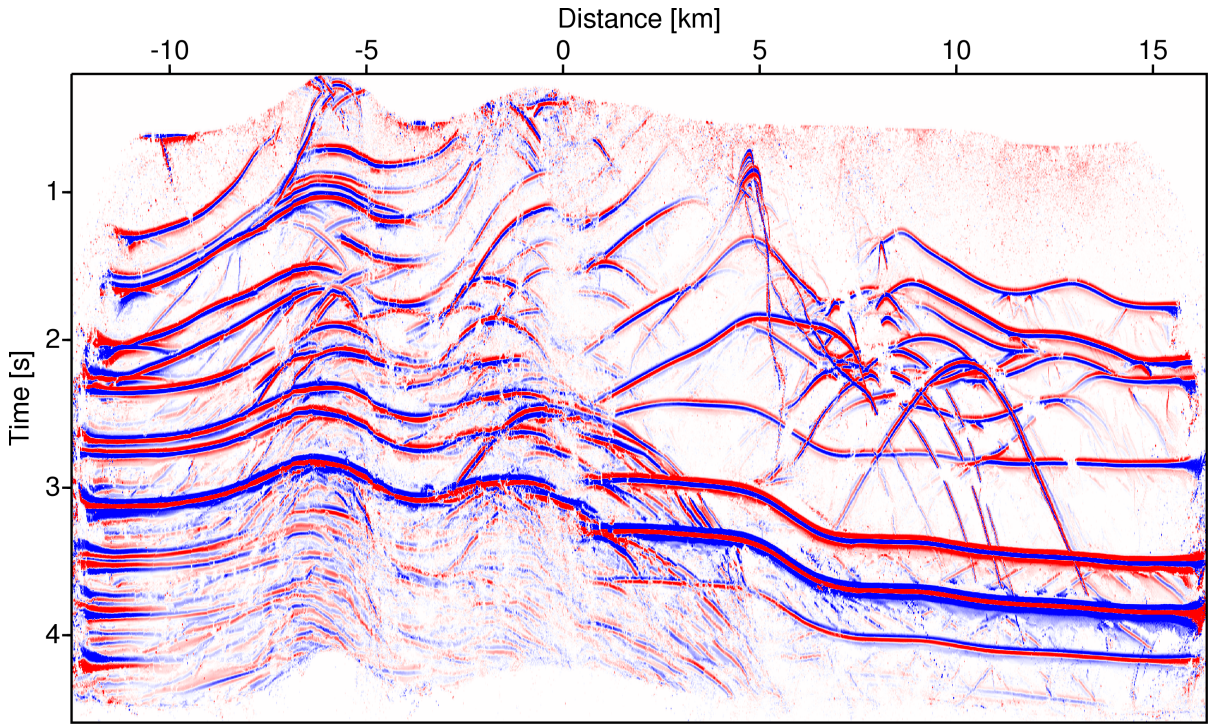

Figure 7: Optimized CRS stack result after application of residual static correction and redatuming. The redatuming procedure relates the simulated ZO traveltimes to a horizontal reference surface at $z = 1460$ m depicted in Figure 4.